

Article

An Experimental Study of Temperature Effect on Properties of Nitride Layers on X37CrMoV51 Tool Steel Used in Extrusion Aluminium Industry

Rafał Hubicki ¹, Maria Richert ^{2,*} and Marcel Wiewióra ²¹ Grupa Kęty S.A. S.A., str. Kościuszki 111, 32-650 Kęty, Poland; rhubicki@grupakety.com² AGH University of Science and Technology, str. Gramatyka 10, 30-067 Kraków, Poland; marcelwiewiora@gmail.com

* Correspondence: mrichert@agh.edu.pl

Received: 31 December 2019; Accepted: 11 May 2020; Published: 17 May 2020



Abstract: The paper concerns the effect of annealing time and temperature on the properties of the nitride layer on X37CrMoV51 tool steel used in the extrusion aluminium industry. Samples made from X37CrMoV51 steel were hardened and tempered, and then nitrided at 530 °C. After nitriding, the samples were annealed in a furnace at 470 °C for 8 h, 12 h, 24 h, 30 h and 60 h, and additionally for 20 h at 270 °C. The samples were tested for structure, hardness and abrasion immediately after nitriding and again after annealing. It was found that annealing the nitrided samples leads to degradation of the nitride layer, accounting for the decrease of hardness. The annealing of the samples at 470 °C, over 12 h causes a decrease in mean hardness value from 1176 HV to 1103 HV, and annealing the samples over 30 h at this temperature leads to a decrease in hardness to 964 HV. The changes in nitrogen content in the white (compound) and diffusion layers and the resulting consequences of changes in phase composition and properties were evaluated. Annealing over 30 h at 470 °C caused the white layer to disappear and the average nitrogen content in the diffusion layer to decrease to the level of about 5–6 at%.

Keywords: nitriding; extrusion dies; hardness; structure

1. Introduction

Nitriding of tool surfaces is one of the most commonly used types of heat treatment of tool steels. The nitriding process increases the hardness of the surface layers as well as resistance to abrasion and corrosion [1–4].

The properties achieved by nitriding may change due to the use of the dies and their annealing. During the extrusion process the die is exposed to high temperatures that affect the surface condition. Before the dies are placed in the press, they are heated, which also affects the condition of the nitride layer.

Dies for extrusion of aluminium alloys are subjected to repeated regeneration by secondary nitriding, which results in multiple high temperature treatments. The need for regeneration results from the abrasion of the nitrided layer from the surface of the calibrating bearing of the dies during their exploitation.

Nitriding consists in diffusing nitrogen into the surface layer of steel. It is carried out in the temperature range 500–650 °C in an ammonia atmosphere. Above 400 °C, the ammonia decomposes according to the $\text{NH}_3 \rightarrow 3\text{H} + \text{N}$ reaction. Atomic nitrogen diffuses into the steel and forms nitride phases. At the temperature of 591 °C, the nitride layer consists of three phases: $\epsilon\text{-Fe}_2\text{N}$ nitride, $\gamma'\text{-Fe}_4\text{N}$ nitride and nitrogen ferrite, which contains 0.01% nitrogen at room temperature. At the temperature of

600–650 °C, the γ phase is formed, which, when slowly cooled down to the temperature of 591 °C, transforms into eutectoid $\epsilon + \gamma'$ [5–9].

The hardness of the nitride layer reaches the level of 1100–1200 HV and should maintain this level when reheated to working temperatures of 500–600 °C. The nitride layer of tempered steel is wear-resistant.

The nitriding process, which lasts from about 20 to 50 h, produces a layer with a thickness of 0.2–0.4 mm. Increasing the nitriding temperature causes an increase in the thickness of the nitride layer, however, it reduces its hardness, which adversely affects the resistance to abrasion. Literature data indicate that lower nitriding temperature favours high hardness of the nitride layer and good resistance against erosion and corrosion resistance [1–3].

The effect of nitrogen presence in the atomic structure of steel is the formation of nitrides and the interstitial location of nitrogen in the crystal lattice. Depending on the concentration of nitrogen, different stoichiometric nitride compositions can be found. Nitrides as compounds, such as titanium nitride [10] or boron nitride [11], are characterized by high hardness and refractory properties, and are used in the production of cutting tool blades, refractory laboratory vessels and protective coatings. Gallium nitride was used in the production of blue laser [12]. Like some oxides, nitrides can absorb hydrogen and are considered for hydrogen storage, e.g., lithium nitride [13].

Depending on the concentration of nitrogen, there are different stoichiometric nitride compositions in steels. Apart from nitrides formed as a result of the connection of nitrogen and iron, such as Fe_2N , and Fe_4N , CrN nitrides are also formed in steels containing chromium [14–19]. The formation of a CrN phase results in the reduction in the corrosion resistance of the nitride layer in chromium-containing steels. The CrN phase is formed during nitriding above 500 °C and occurs frequently when using traditional methods of nitriding [1,2]. CrN precipitations, dissolved in ferrite, are very hard. The temperature increase causes them to undergo coalescence, which leads to the loss of coherence with the lattice, and the decrease in hardness, as well as initiate changes in the profile of long-range internal stresses. These changes already take place during nitriding.

Depending on the nitrogen content, iron nitride phases with different structure and properties can be formed. Iron has five nitrides observed at ambient conditions, Fe_2N , Fe_3N_4 , Fe_4N , Fe_7N_3 and Fe_{16}N_2 [15,19,20]. They are crystalline, metallic solids. Lately, it was put forward that the phase diagram of iron nitrides can be extended further, to even more N-rich compounds, such as the γ'' -FeN and the γ''' -FeN phases [21].

All iron nitrides are metallic conductors and they are metastable with respect to decomposition into Fe and N_2 . The decomposition is limited by kinetic barriers. Atomic nitrogen can be dissolved in the body-centred cubic (bcc) lattice of α -Fe to a concentration of about 0.4 at% N without much distortion of the lattice. When more than 2.4 at% N is dissolved in pure Fe, the bcc lattice undergoes a tetragonal deformation. In the composition range up to about 11 at% N, the iron nitride compound is called nitrogen martensite α' . This phase has a body-centred tetragonal (bct) structure with lattice parameters depending on the nitrogen content. The N atoms occupy randomly octahedral hollow sites in the Fe sublattice. At saturation, nitrogen martensite has the Fe_8N composition. The α' - Fe_8N can transform into the α'' - Fe_{16}N_2 phase. In this phase, the N atoms are ordered. It can be formed under special conditions from Fe, however, not in its pure form. The α'' - Fe_{16}N_2 phase attracted considerable attention because of a possible very high saturation magnetization, reported to vary between 2.4 T and 3.2 T [16]. The next phase of the nitrogen content is the γ' - Fe_4N phase (roaldite), which is cubic, with the Fe sublattice arranged in a face-centred cubic (fcc) structure and nitrogen atoms occupying the body-centred position 1/4. As indicated in the phase diagram, this phase has a narrow composition range around 20 at% N. The lattice parameter is 3.795 Å and the saturation magnetization was reported to be between 1.8 T and 1.9 T [17]. A saturation magnetization value in this range is slightly lower than the one of pure iron (2.21 T), making this phase somewhat less attractive in comparison with Fe.

The authors of the paper [21] point to the important role of carbon in the process of phase changes in the nitride layer and its influence on the internal stress in this zone. Carbon diffusion implies

a complex precipitation sequence and thermodynamical evolution that modify the volume change during nitriding. The transformation of initial carbides into nitrides decreases the kinetics of nitriding and is counteracted by the precipitation of cementite. Surface decarburization involves a decrease in the volume fraction of cementite during nitriding, leading to an unloading of the surface and thus reducing residual stresses. During nitriding, a surface was subject to mechanical loading–unloading through volume changes. The distribution of residual stresses is mainly governed by the thermochemical modifications due to nitrogen and carbon diffusion.

Studies show that the abrasion resistance of the nitride layer depends on the type of nitriding method [22]. Studies by G. Kugler et al. [23] have shown that the presence of a compound (white) layer protects the surface of dies against chemical reaction with hot aluminium [24]. It was found that annealing of the ϵ -Fe₃N phase leads to the precipitation of the γ' -Fe₄N phase. In this paper it was also found that long annealing of ϵ phase causes its homogenization.

In general, it should be emphasized that any exposing a surface-nitrided tool to high temperatures leads to changes in the nitride layer. In combination with the changes that occur in the substrate, consisting in lowering the density of defects (recovery, polygonization) and the precipitation or decomposition of carbides, as well as their coagulation, this affects the properties of the nitride layer. In particular, the hardness and abrasion resistance of the nitrided surface change. Reducing these properties reduces the life of the dies and increases production costs.

The scope and scale of changes affecting the durability of the dies is of crucial importance due to the practice of using the dies in industry. From this point of view, the more stable the hardness of the nitrided layer is, the better the prognosis of the durability and utility of the die.

Continuous development of the aluminium market causes the demand for dies to increase. According to the prediction of the International Energy Agency, between 2023 and 2030, the demand for aluminium will increase by more than 50 percent, due to, among other things, the rapid development of LED lighting and the development of the automotive industry [25]. The largest aluminium products' production plant in Poland is Grupa Kęty S.A. S.A., which is a company with a long tradition [11]. Grupa Kęty S.A. assumes that, by 2019, it will become the leader in the production of aluminium profiles in Poland with sales of 1 364 million PLN in the Polish aluminium market [26].

The development of the aluminium industry generates the development of production and heat treatment of dies necessary for the production of aluminium profiles. Due to the importance of the die durability issue, the nitriding process is constantly being improved by companies producing nitriding furnaces. Therefore, all research on this subject contributes to the broadening of the knowledge on this subject and to the improvement of the nitriding technology.

In this paper the influence of temperature on the properties of the nitride layer of tool steel X37CrMoV51 (1.2344 tool steel) was analysed. Annealing was carried out for different time periods (8–60 h) and the influence of the given heat treatment conditions on the structural effects and properties of the nitride layer was evaluated.

2. Materials and Methods

The tested samples were nitrided in a Nitromax furnace under industrial conditions.

Samples made from X37CrMoV51 steel were hardened and tempered, and then nitrided at 530 °C, according to Grupa Kęty S.A.'s (Kęty, Poland) proprietary technology based on the NITREG technology, under conditions in which industrial dies in Grupa Kęty S.A. S.A. are nitrided. During primary nitriding, a 120 to 140 μ m thick diffusion layer should be formed on the dies. The thickness of the white layer should be between 4 and 6 μ m and the hardness should be higher than 1000 units.

After nitriding, the samples were annealed in a furnace at 470 °C for 8 h, 12 h, 24 h, 30 h and 60 h, and additionally for 20 h at 270 °C. The samples were tested according to the following procedures for structure, hardness and abrasion resistance immediately after nitriding and again after annealing.

The research was carried out on cross sections. After cutting out the sample, it was sanded with grade #300 and #1200 abrasive papers and polished with diamond paste with grain sizes of 9 μ m, 3 μ m

and 1 μm . The final polishing was carried out using the silica suspension OP-S according to Struers company procedures. In the next step, the samples were etched in Nital reagent with the following composition: 5 mL HNO_3 + 100 mL $\text{C}_2\text{H}_5\text{OH}$.

The microstructure of the samples was examined using the Olympus GX-51 optical microscope (Cracow, Poland) and the Hitachi SU-70 scanning electron microscope (Cracow, Poland) equipped with Energy Dispersive X-Ray Analysis (EDX).

The microhardness of the nitride layer was examined using the Shimadzu HMV-G apparatus (Cracow, Poland) by means of Vickers' method with the load of 0.9807 N.

Chemical analyses in the microarea of nitrided steel and iron oxides formed as a result of gas nitriding were carried out using an electron probe microanalyser Jeol SuperProbe JXA-8230 (Cracow, Poland) equipped with Wavelength Dispersive X-ray analysis (WDS). The tests were performed in the Critical Elements Laboratory of AGH-KGHM at the Faculty of Geology, Geophysics and Environmental Protection of the AGH University of Science and Technology in Krakow. Investigations of nitrided steel were carried out with the use of an electron probe microanalyser with the acceleration voltage of 15 kV and the amperage of 50 nA, whereas, during the measurements of iron oxides, the amperage was 40 nA. The time of analysis of each element lasted 20 s in peak maximum position and 10 seconds in background position before and after the peak. The beam size was $<1 \mu\text{m}$. The following lines and standards were used for steel analysis: BN ($\text{NK}\alpha$), Fe ($\text{FeK}\alpha$), Mo ($\text{MoL}\alpha$), V ($\text{VK}\alpha$), Cr ($\text{CrK}\alpha$). The following lines and standards were used for the analysis of iron oxides: BN ($\text{NK}\alpha$), fayalite ($\text{FeK}\alpha$), Mo ($\text{MoL}\alpha$), V ($\text{VK}\alpha$), Cr_2O_3 ($\text{CrK}\alpha$).

3. Results

Studies on the structure of samples directly after nitriding showed that a white (compound) layer was formed on their surface (Figure 1). The thickness of this layer was estimated at about 7–8 μm , while the depth of the diffusion layer was about 70 μm (Figure 1).

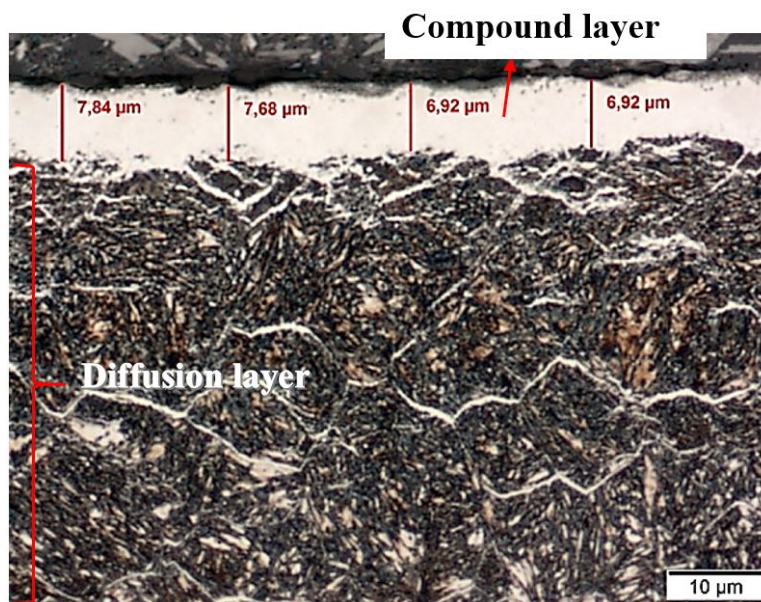


Figure 1. White layer in nitrided Nitromax furnace samples; microstructure of 1.2344 tool steel after gas nitriding shown through an optical microscope; white layer thickness $\sim 7 \mu\text{m}$, diffusion layer $\sim 70 \mu\text{m}$.

To estimate the nitrogen content in the studied layers the EDX method of chemical composition analysis with a scanning microscope was applied. The locations where the chemical composition was determined are shown in Figure 2 and quantitative results of chemical composition tests are shown in Table 1. The high nitrogen level and structural phase contrast identified a white (compound) layer.

The white layer contained more than 21 at%. of nitrogen, which means the range of occurrence of $\gamma' + \epsilon$, or $\epsilon\text{-Fe}_2\text{N}$ nitride, $\gamma'\text{-Fe}_4\text{N}$ nitride and nitrogen ferrite, which contains 0.01% nitrogen at room temperature (Figure 3). Table 1 also shows results indicating the presence of a diffusion layer with nitrogen in the range 3.9–7.2 at%. These values indicate the extent of the presence of eutectoid mixture $\alpha + \gamma'$ consisting of phases: $\gamma'\text{-Fe}_4\text{N}$ nitride and α -nitride ferrite.

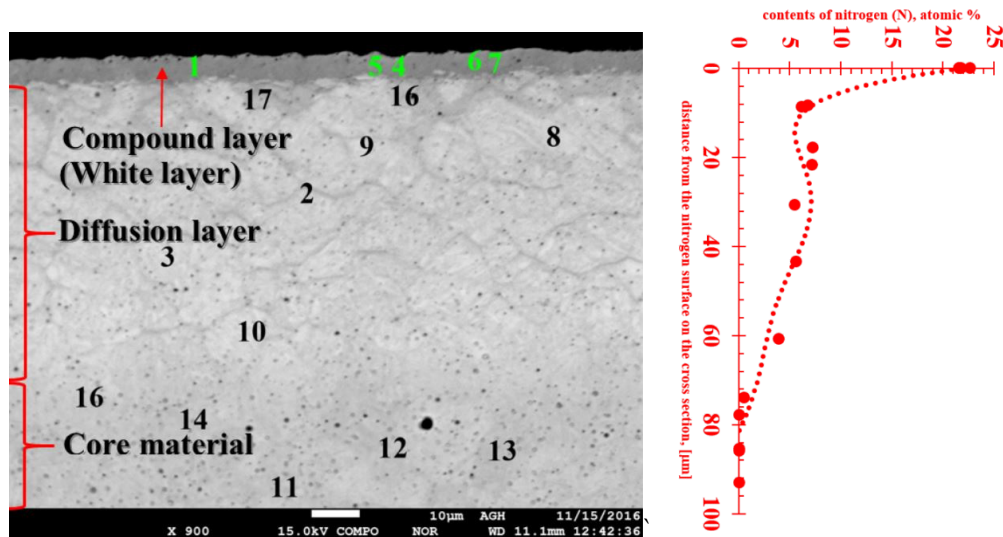


Figure 2. Point analysis of the chemical composition of: the white layer—points 1, 4–7; the diffusion layer—points: 2, 3, 8, 9, 10, 16, and 17; and the steel matrix—points 11–14 in 1.2344 steel after gas nitriding.

Table 1. Results of chemical composition analysis in the points marked in Figure 2.

	N	Mo	Fe	V	Cr	Kind of Nitride Layer
Atomic %						
2	5.442	0.697	84.946	0.961	5.237	Diffusion layer
3	5.532	0.703	85.036	0.980	5.432	
4	21.702	0.499	70.824	0.582	4.606	
5	21.563	0.557	70.355	1.220	4.572	Compound layer (white layer)
6	22.615	0.488	69.383	0.627	5.062	
7	21.513	0.514	71.019	0.577	4.587	
8	7.201	0.601	83.927	0.727	5.295	Diffusion layer
9	7.117	0.597	84.045	0.698	5.256	
10	3.823	0.693	86.829	0.780	5.528	
11	0.000	0.695	90.185	0.887	5.829	Core material
12	0.000	0.710	90.165	0.961	5.750	
13	0.000	0.721	90.287	0.901	5.635	
14	0.000	0.717	90.171	0.906	5.797	Boundary between diffusion layer and core material
15	0.452	0.737	89.747	1.009	5.709	
16	6.698	0.583	84.632	0.761	5.264	Diffusion layer
17	6.117	0.635	84.690	0.715	5.684	

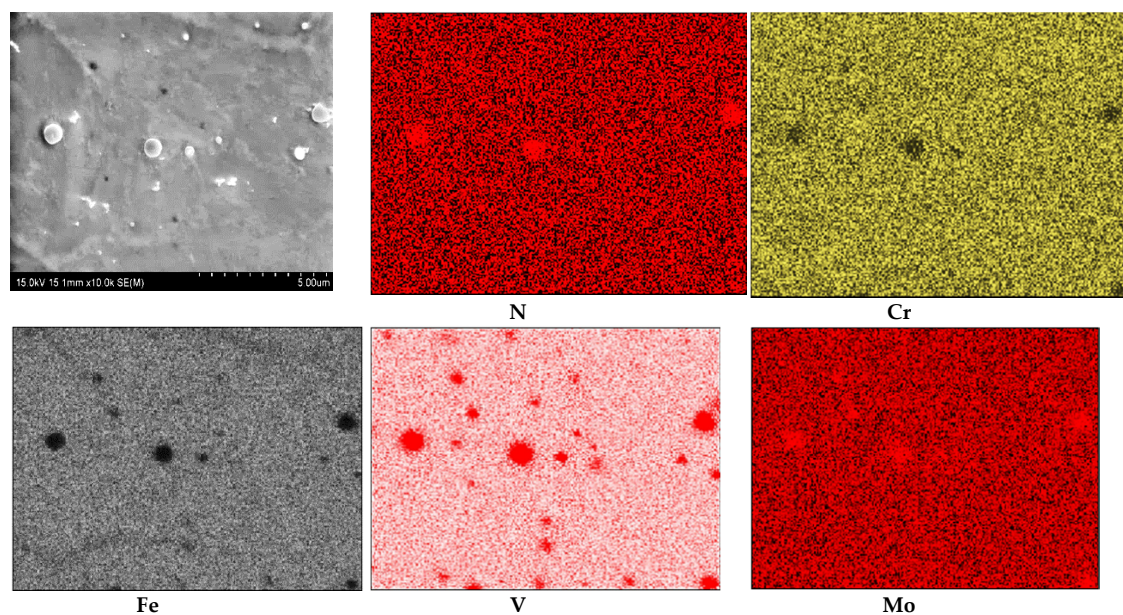


Figure 3. Map of elemental distribution in the white layer of the nitrided sample.

The nitrogen profile attached to Figure 2 clearly shows that the very high nitrogen content in the near-surface layer decreases rapidly and already at a distance of about 10 μm from the sample surface, then at a distance of about 80 μm it reaches the zero level. This is the indicator of the boundary of the diffusion layer. Therefore, the thickness of the hard, nitride layer is relatively small, and the friction forces cause its rapid wear, which makes it necessary to regenerate the layer after a specified period of using the tool.

The results of WDS analysis of the chemical composition of the white layer (compound layer) in the form of elemental distribution maps are presented in Figure 3. In the maps, the position of nitrogen concentration appeared at the same place as the position of Fe, Cr, V and Mo. The average nitrogen content in the white layer was about 21.84 at% and in the diffusion layer it was about 5.82 at%. The average in both layers' content of nitrogen was found to be 13.82 at%. The Cr content was estimated in white layer at about 4.71 at%, in the diffusion layer at about 5.35 at% and in the core material at about 5.75 at%—for an average value of about 5.27 at%. The content of Mo in the white layer was about 0.51 at%, in the diffusion layer about 0.66 at% and in the core material 0.71 at%. Generally the content of Mo was 0.63 at%. The V content in the white layer was about 0.75 at%, in the diffusion layer 2.03 at% and in the core material about 1.14 at%. The average V content was about 1.31 at%.

The existence of Cr, V and Mo in the same positions on the chemical composition maps from WDX measurement (Figure 3) suggests the probability of complex nitride precipitation. In such a case, chromium surely is dissolved in iron nitrides. It was shown that in ternary alloy systems where the crystal structures of the binary boundary nitrides are similar and the interaction parameter difference of the nitride forming elements is moderate, mixed ternary nitrides can develop [27]. Increasing numbers of ternary nitrides, $A_xM_yN_z$, have been described in recent years, and these exhibit a great richness of structure and physical property [28,29].

After nitriding, the samples were annealed at 470 $^{\circ}\text{C}$ for 3 h (Figure 4a,b), 8 h (Figure 5a,b), 30 h (Figure 6a,b) and 60 h (Figure 7a,b). As a result of annealing, the white layer was degraded. Microstructure observations show that the thickness of the white layer decreased as the annealing time increased, and for the annealing time of 30 h and 60 h it disappeared altogether.

The width of the diffusion layer was observed to grow and equalled about 70 μm for 3 h and 8 h of annealing, about 80 μm for 30 h and about 100 μm for 60 h.

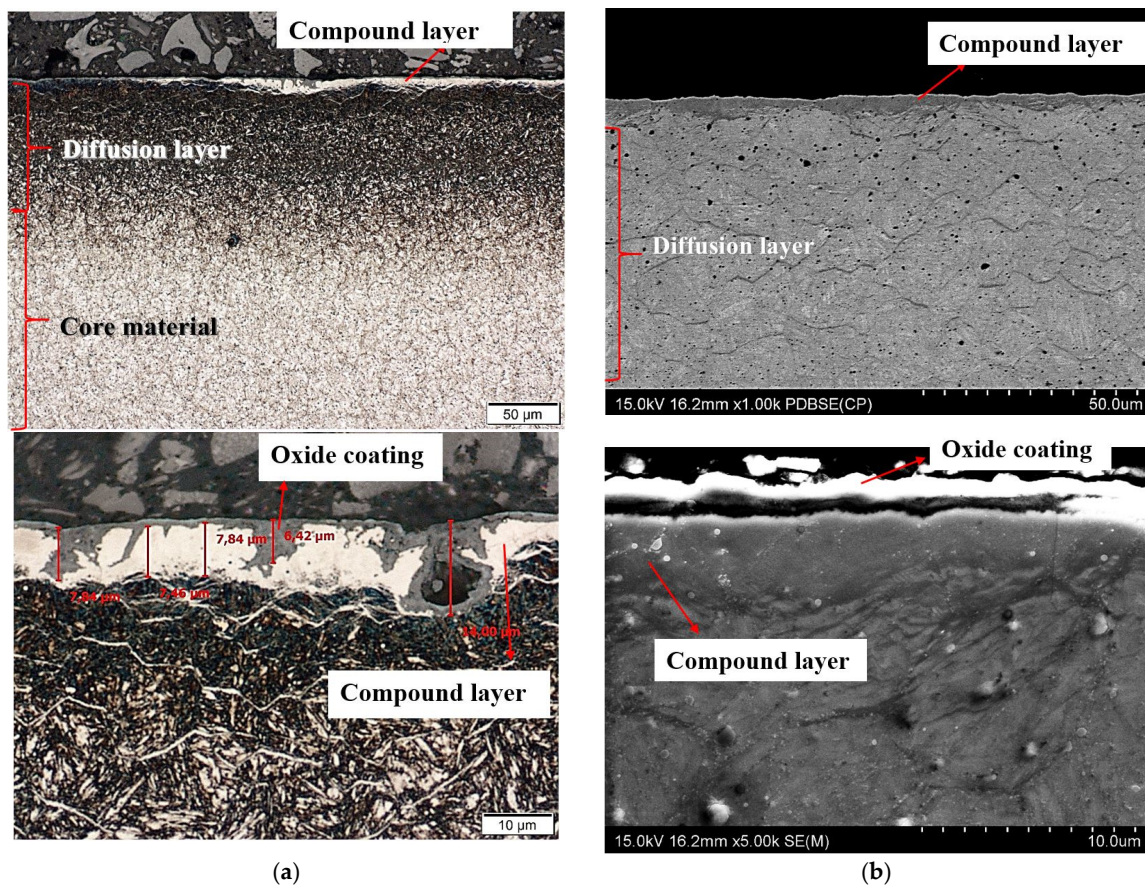


Figure 4. (a) Microstructure of WCLV steel after gas nitriding at Grupa Kęty S.A. and annealing for 3 h at 470 °C, show through an optical microscope (OM). Thickness of white layer $\sim 7 \mu\text{m}$ and diffusion layer $\sim 70 \mu\text{m}$. Visible on the surface is the corrosive layer formed during annealing which results in degradation of the white layer (b) Microstructure of WCLV steel after gas nitriding in Grupa Kęty S.A. and annealing for 3 h at 470 °C, shown though a scanning microscope (SEM). Thickness of white layer $\sim 7 \mu\text{m}$, diffusion layer $\sim 70 \mu\text{m}$ and corrosion $\sim 2 \mu\text{m}$.

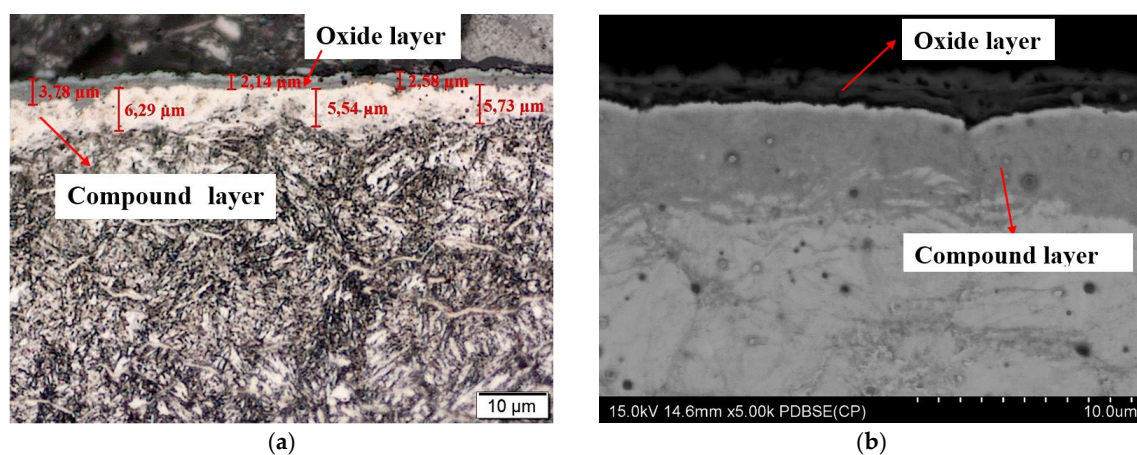


Figure 5. (a) Microstructure of WCLV steel after gas nitriding in Grupa Kęty S.A. and annealing for 8 h at 470 °C, shown with an optical microscope. Thickness of the white layer $\sim 6 \mu\text{m}$, diffusion layer $\sim 70 \mu\text{m}$ and corrosion layer $\sim 2 \mu\text{m}$. The corrosion layer visible on the surface was formed during annealing, and it causes degradation of the white layer. (b) Microstructure of WCLV steel after gas nitriding in Grupa Kęty S.A. and annealing for 8 h at 470 °C, shown with a scanning microscope. Thickness of white layer $\sim 6 \mu\text{m}$, diffusion layer $\sim 70 \mu\text{m}$ and corrosion layer $\sim 2 \mu\text{m}$.

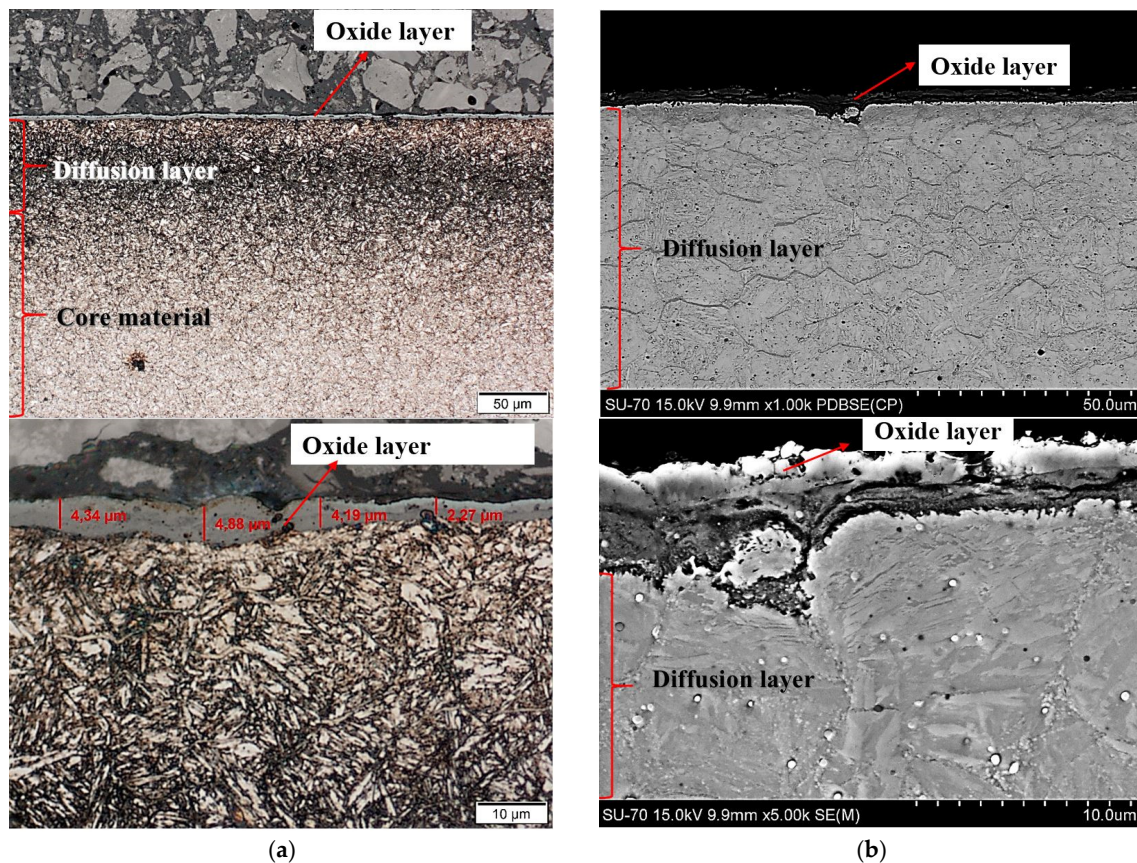


Figure 6. (a) Microstructure of WCLV steel after gas nitriding in Grupa Kęty S.A. and annealing for 30 h at 470 °C, shown with an optical microscope. No visible white layer. Layer thickness of diffusion layer $\sim 80 \mu\text{m}$ and corrosion layer $\sim 4 \mu\text{m}$. (b) Microstructure of WCLV steel after gas nitriding in Grupa Kęty S.A. and annealing for 30 h at 470 °C, shown with a scanning microscope. No white layer. Layer thickness of diffusion layer $\sim 80 \mu\text{m}$ and corrosion layer $\sim 4 \mu\text{m}$.

The oxidation of nitride samples appeared locally after annealing for 3 h at 470 °C (Figure 4a) and increased with annealing time prolongation. The oxide growth at temperatures between 423 K and 623 K could be described consistently with the oxidation model of Fromhold and Cook (FC) [30]. It describes the initial oxidation of metals (0–20 nm). In the FC theory, the reaction between metal and oxygen takes place at the growing oxide/oxygen interface, requiring both metal ions and electrons to move through the oxide layer to the surface. The transport of electrons can proceed by two mechanisms: tunnelling and thermionic emission. For temperatures below 420 K, there is virtually no thermionic emission at the metal–oxide interface, and electron tunnelling is the dominant process. According to the FC formalism, at $T \leq 420 \text{ K}$, electron transport proceeds by tunnelling through the oxide layer and therefore the limiting film thickness should be nearly independent of the oxidation temperature. However, the measurements show that the saturation thickness does depend on the temperature and varies between $8.5 \times 10^{15} \text{ O atoms/cm}^2$ at room temperature (RT) and $15 \times 10^{15} \text{ O atoms/cm}^2$ at 395 K [31,32]. A two-layer system is formed, with a first layer containing Fe^{2+} only, and a top layer containing both Fe^{3+} and Fe^{2+} . The growth of the second layer starts at an oxygen coverage of $4.0 \times 10^{15} \text{ O atoms/cm}^2$ and consists of $\text{Fe}_{0.77}\text{O}$ (which is probably a mixture of FeO and $\gamma\text{-Fe}_2\text{O}_3$). At higher oxidation temperatures, the relative fraction of Fe^{3+} in the formed oxide decreases. The oxide layer formed in O_2 at 473 K consists of Fe^{2+} only. The decrease of the oxidation rate coincides with the formation of an oxide layer containing Fe^{3+} . Upon annealing, Fe^{3+} is reduced to Fe^{2+} , while the displaced Fe^0 is oxidized to Fe^{2+} . For larger oxide thicknesses ($L > 3 \text{ nm}$) and higher temperatures ($T > 420 \text{ K}$), the dominant electron transport processes thermionic emission. For higher temperatures and larger

oxide thicknesses, the thermionic emission of electrons is rate-limiting. For lower temperatures and smaller oxide thicknesses the presence of Fe^{3+} drastically decreases the oxidation rate. The reduction rate of Fe^{3+} to Fe^{2+} increases with increasing temperature. An important feature of the FC theory is the concept of coupled currents: the net electrical current across the oxide layer is zero. At sufficiently high oxygen pressures, transport of either electrons or metal ions is rate-limiting.

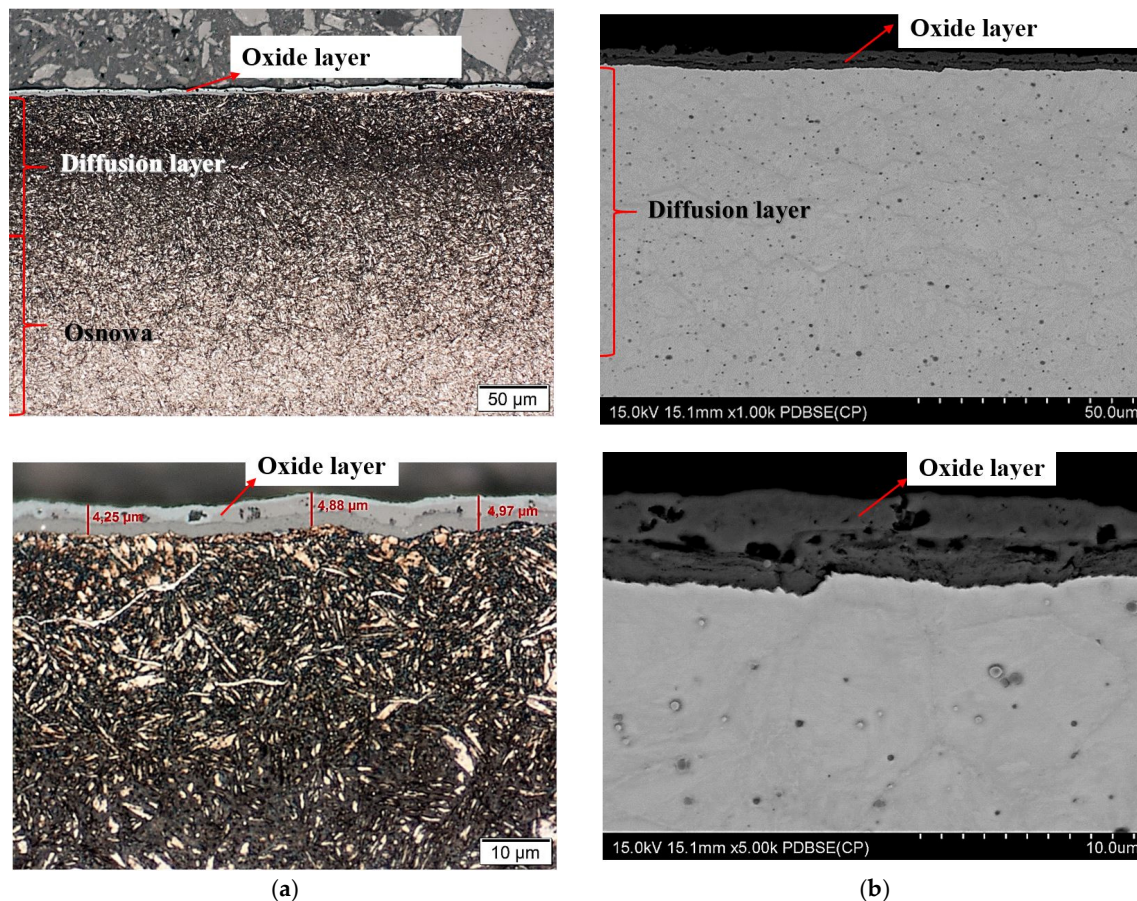


Figure 7. (a) Microstructure of WCLV steel after gas nitriding in Grupa Kęty S.A. and annealing for 60 h at 470 °C, shown with an optical microscope. No white layer. Layer thickness of diffusion layer ~100 μm and corrosion layer ~4.5 μm. (b) Microstructure of WCLV steel after gas nitriding in Grupa Kęty S.A. and annealing for 60 h at 470 °C, shown with a scanning microscope. No white layer. Layer thickness of diffusion layer ~100 μm and corrosion layer ~4.5 μm.

The oxidation of nitride steel was investigated by Yang Li and all [33]. The iron oxide phases of hematite (Fe_2O_3) and magnetite (Fe_3O_4) through the post-oxidizing treatment at 400 °C and 450 °C was found. The hematite has been also identified in work [34] after the postoxidation of plasma nitriding AISI 4140 steel. In contrast, in [35], after oxidation of nitride layer at 480 °C to 500 °C, Fe_3O_4 (magnetite) was reported. It was also described that the precipitation of CrN or Cr in complex nitride precipitations at 500 °C removed Cr from the solid solution and adversely affected the oxidation performance at this temperature [35]. Formation of CrN and γ' - Fe_4N , causes the corrosion resistance of the nitrided layer to decrease [36]. The nitrogen atoms occupy similar types of surface sites as the oxygen atoms [37] Displacement of N atoms from the surface into the bulk by interaction with gaseous O_2 will be energetically rather favourable. The bulk diffusion coefficient of N in pure Fe has, at 900 K, a value of about $10^{-7} \text{ cm}^2/\text{s}$ and an activation energy of 18.9 kcal/mole. Extrapolation to room temperature yields a mean displacement by diffusion of about 5 Å within 30 min. This process will, however, certainly be strongly accelerated by the rearrangement of the Fe atoms in the course of oxide

formation (oxygen chemisorption on Fe(100)), which was found to cause an expansion of the topmost layers, as well as by the energy release associated with the oxygen attack so that displacement of the N atoms even at room temperature becomes feasible. On the other hand, the further growth of the oxide will certainly be retarded by previous formation of a nitride layer in the surface region—this is the well-known anticorrosive effect.

The research showed that, as a result of long annealing times, the surface hardness of the samples decreased by about 200–250 units (Figure 8) in relation to the hardness of the original nitrided sample. The hardness results shown in Figure 8 can be divided into three groups, as presented at Figure 9. The highest hardness (average 1176 HV) is found in samples annealed for 3, 8 and 12 h at the temperature of 470 °C. The group of samples annealed for 20 h at 270 °C have the average hardness 1103 HV. The lowest hardness was found in samples annealed for 30 and 60 h at 470 °C with the average hardness 964 HV. The difference between the highest and lowest hardness is 212 HV.

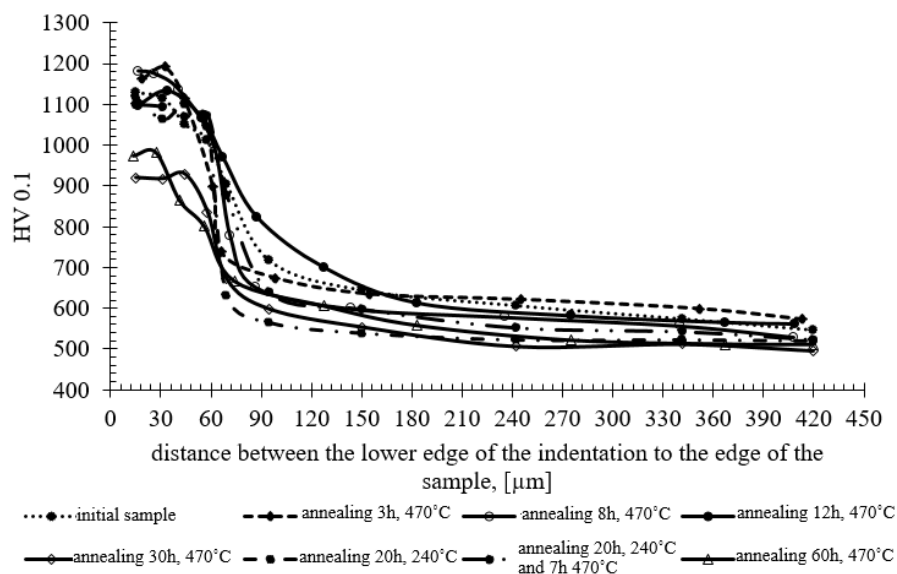


Figure 8. Hardness change profiles as a function of annealing time at 470 °C.

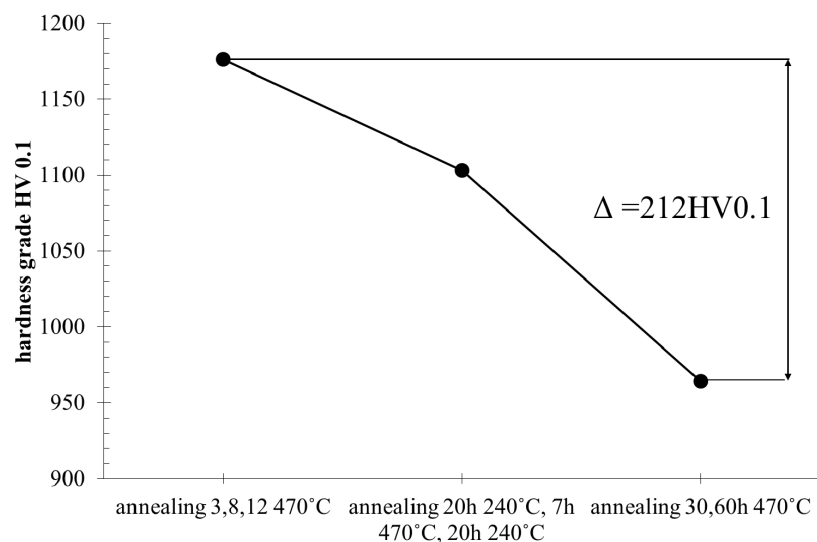


Figure 9. Mean hardness graph of three groups of annealed nitrided WCLV steel samples, measured at 15 μm from the sample surface. HV = 1176—mean hardness of sample group annealed at 3, 8 and 12 h at 470 °C; HV = 1103—mean hardness of sample group annealed for 20 h at 240 °C, 7 h at 470 °C and 20 h at 240 °C; and HV = 964—mean value of hardness for annealing at 30 h and 60 h at 470 °C.

Abrasion tests revealed a correlation between the hardness level and weight loss in the abrasion test. It was found that the lower the hardness, the more abrasive the surface of the samples was (Figure 10).

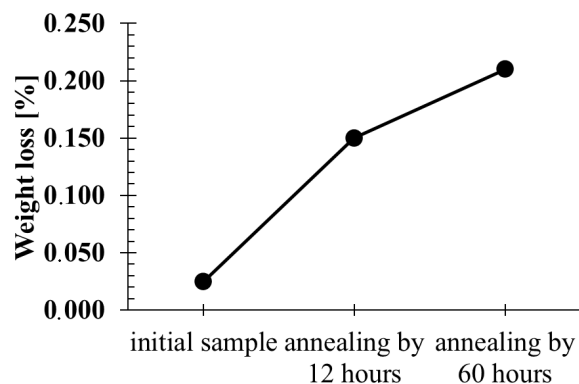


Figure 10. The weight loss of initial sample (0.025), sample annealed for 12 h in 470 °C (0.15) and samples annealed for 60 h at 470 °C (0.21).

The analysis of nitrogen content in the white and diffusion layers was based on the results of EDX and WDS chemical composition tests. Figure 11 summarizes the data on nitride content in white and diffusion layers. The white layer contained on average about 19.4% atomic of nitrogen and this level of nitrogen is stable in samples annealed in the range of 3 to about 12 h at 470 °C. Above this time of annealing, the white layer disappeared. For the annealing times of 30 h and above, no white layer was found. The nitrogen content in the white layer suggests the occurrence of $\gamma' + \epsilon$ phases. When the content of nitrogen decreases, the aforementioned phases do not exist. It should be assumed that the disappearance of the white layer occurred as a result of the decrease in nitrogen content, which diffused deep into the substrate, as evidenced by the increase in the thickness of the diffusion layer.

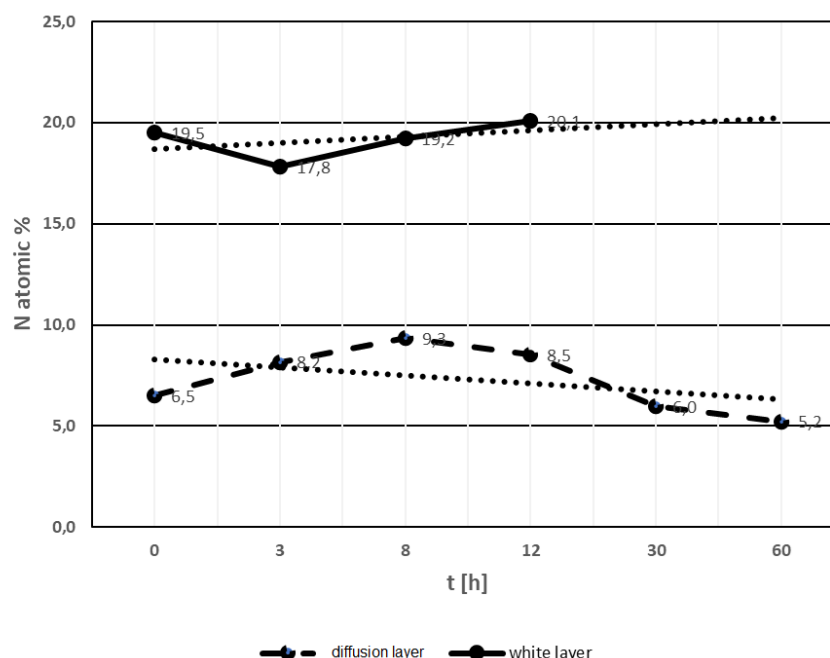


Figure 11. Mean nitrogen content in the white and diffusion layer in the samples after nitriding and annealing for 3–60 h at the temperature of 470 °C, measured at the same place from surface. The upper line shows mean value of nitrogen in white layer. The dotted line indicates estimation course in annealing time. The lower line indicates mean value of nitrogen content in diffusion layer and the dotted line indicates the tendency to decreasing nitrogen content with the extension of annealing time.

The diffusion layer contained about 8.1% atomic of nitrogen in samples annealed for 8–12 h (Figure 11). Samples annealed for more than 12 h showed an average nitrogen content reduced to about 5.6% atomic. Reduced nitrogen content in the diffusion layer predicted the presence of phases $\alpha + \gamma'$.

4. Discussion

Coatings and layers produced by various surface engineering methods reveal a variety of structures and thicknesses. This is due to the mechanisms of forming coatings and layers. Nitriding is a specific surface treatment in which the top layer of a tempered tool is saturated with nitrogen at high temperatures. The effect of nitrogen in the atomic structure of steel is the formation of nitrides and the interstitial location of nitrogen in the crystal lattice. Depending on the concentration of nitrogen, different stoichiometric nitride compositions can be found. Apart from nitrides formed as a result of the compound of nitrogen and iron, i.e., nitrides such as Fe_2N and Fe_4N , moderate mixed ternary nitrides can also develop. In the conducted studies the searching of nitride particles were performed by EDX and WDS measurement of chemical composition in points and chemical composition maps. We found Cr, Mo, Fe, V and N concentration in the same places, which suggests formation in or quaternary phase [38,39]. The investigation in work shows that at lower Cr/Mo ratio, hexagonal CrMoN_2 precipitation occurred.

The presence in the nitride test layer of a hard nitrogen phases occur near the surface of the samples is significant for die resistance to abrasion. Nitrogen phases especially increase the hardness, which translates into higher abrasion resistance [40]. Reducing the surface nitrogen content in the white layer leads to phase changes and loss of high hardness [41,42]. As a result of experimental annealing, the initial hardness of the nitride layer, amounting to approximately 1190HV, was reduced by approximately 210 units (Figure 8). From a practical point of view, reducing the hardness below 1000HV disqualifies aluminium extrusion dies for further use. During the annealing at 470 °C, the oxidation of the sample surface develops. The thickness of the oxide layer increases with annealing time prolongation. However, above 8 h of annealing, it becomes almost stable. Experimental investigations show a “parabolic law” of oxide layer growth [43]. Dwivedi D., Lepková K. and Becker T. [44] point out on the importance of texture in the corrosion process. Robert E. Melchers [45] presented different models of corrosion loss starting from different assumptions and showed parabolic and linear laws of oxidation. The oxidation zone containing (Mn,Fe)O and (Mn,Cr,Fe) $_3\text{O}_4$ oxides in annealed Fe–1.9Mn–1.6Cr steel was investigated by Mao, W., Ma, Y. and Sloof, W.G [46]. It was found that the penetration depth of oxides along grain boundaries is much larger (by a factor of two or more) than that of internal oxides formed inside grains. They also found a parabolic rate law of oxidation. In relation to obtained results, it should be assumed that the parabolic oxide layer grows and oxidation stabilizes in the range of 30 h to 60 h of annealing.

It should be mentioned that the presence of nitride and carbide phases in tools for which no additional heat treatment is applied is beneficial due to the high surface hardness. However, if the surface of the die is designed to be covered with an additional coating, e.g., PVD - Physical Vapour Deposition, the heat treatment should be carried out in such a way that no white layer is formed. There should only be a diffusion zone characterized by maximum effective thicknesses and devoid of carbide precipitations at the grain boundaries of the former austenite [42]. It can therefore be concluded that the design and implementation of the nitriding process and its effects will depend on the purpose for which the tools are used.

The life cycle of the dies includes periods at elevated temperatures (470 °C and 520 °C) and periods at room temperature. Cyclic changes in the working temperature during die life of the die make it subject to processes of structural and phase changes. This results in changes of properties and ultimately, after the loss of the required hardness level, the need for regeneration through secondary nitriding.

The substrate is also subject to changes under the influence of temperature. There are recovery processes that reduce dislocation densities and other lattice defects. The processes of precipitation coagulation take place. Precipitations that were coherently bound to the matrix lose their coherence,

which results in a decrease of hardness. The phenomena of structure restoration, combined with changes in the morphology of the precipitations, lead to unfavourable changes of properties in terms of die exploitation.

5. Conclusions

On the basis of the research carried out, it was found that:

1. Annealing of the nitrided samples leads to degradation of the nitride layer and the decrease of hardness.
2. It was found that annealing of the samples at 470 °C, over 12 h causes a decrease in mean hardness value from 1176 HV to 1103 HV and annealing the samples over 30 h at this temperature leads to a decrease in hardness to 964 HV.
3. Tests have shown a decrease in abrasive resistance as the annealing time increases.
4. Annealing over 30 h at 470 °C caused the white layer to disappear and the average nitrogen content in the diffusion layer to decrease to the level of about 6 at%.

Author Contributions: Conceptualization, R.H., M.R. and M.W.; Investigations R.H., M.R. and M.W., Writing-Original Draft: M.R., Preparation, R.H., M.R. and M.W. All authors have read and agreed to the published version of the manuscript.

Funding: This research received no external funding.

Acknowledgments: This work was supported by the subsidies for the maintenance and development of research potential of AGH University.

Conflicts of Interest: The authors declare no conflict of interest.

References

1. Yang, M. Nitriding—Fundamentals, Modeling and Process Optimization. Ph.D. Thesis, Worcester Polytechnic Institute, Worcester, MA, USA, April 2012.
2. Conceição Rocha Lima Cesconetto, M.; Ribeiro Franco, A., Jr.; Aparecido Vieiraa, E. Improving the Abrasive Wear Resistance of a Microalloyed Steel by Plasma Nitriding. *Mater. Res.* **2015**, *18*, 334–340. [CrossRef]
3. Aydin, H.; Bayram, A.; Topcu, S. The effect of duplex surface treatment on erosion performance of QRO 90 Supreme steel. *Mater. Sci.* **2013**, *19*, 19–24.
4. Xu, X.; Wang, L.; Yu, Z.; Qiang, J.; Hei, Z. Study of microstructure of low-temperature plasma nitride AISI 304 stainless steel. *Metall. Mater. Trans. A* **2000**, *21A*, 1193–1199. [CrossRef]
5. Kooi Bart, J.; Somers Marcel, A.J.; Mittemeijer Eric, J. An Evaluation of the Fe-N Phase Diagram Considering Long-Range Order of N Atoms in γ' -Fe₄N_{1-x} and ϵ -Fe₂N_{1-z}. *Metall. Mater. Trans. A* **1996**, *27A*, 1063–1071. [CrossRef]
6. Eom, J.Y.; Shankar Rao, V.; Kwon, H.S.; Nam, K.S. Experiments and modeling study on growth behavior of Cr-nitrides formed on electroplated hard Cr during ion-nitriding. *J. Mater. Res.* **2003**, *18*, 861–867.
7. Widenmeyer, M.; Hansen, T.C.; Meissner, E.; Niewa, R. Formation and Decomposition of Iron Nitrides Observed by in situ Powder Neutron Diffraction and Thermal Analysis. *J. Inorg. Gen. Chem.* **2014**, *640*, 1265–1274. [CrossRef]
8. Bjørnsom, H.B. Investigation of the Compound Layer and Diffusion Zone of Pulsed Plasma Nitrided 51CrV4-Steel. Master's Thesis, Energy and Nanotechnology Department of Physics, University of Oslo, Oslo, Sweden, September 2013. Available online: https://www.duo.uio.no/bitstream/handle/10852/41371/Bjorsom_Masteroppgave.pdf?sequence=1 (accessed on 30 September 2013).
9. Díaz-Guillén, J.C.; Vargas-Gutiérrez, G.; Granda-Gutiérrez, E.E.; Zamarripa-Piña, J.S.; Pérez-Aguilar, S.I.; Candelas-Ramírez, J.; Álvarez-Contreras, L. Surface Properties of Fe₄N Compounds Layer on AISI 4340 Steel Modified by Pulsed Plasma Nitriding. *J. Mater. Sci. Technol.* **2013**, *29*, 287–290. [CrossRef]
10. Van Hove, R.P.; Sierevelt, I.N.; van Royen, B.J.; Nolte, P.A. Titanium-Nitride Coating of Orthopaedic Implants: A Review of the Literature. *J. List Biomed. Res. Int.* **2015**, *2015*, 485975. [CrossRef]
11. Caldwell, J.D.; Aharonovich, I.; Cassaboiss, G.; Edgar, J.H.; Gil, B.; Basov, D.N. Photonics with hexagonal boron nitride. *Nat. Rev. Mater.* **2019**, *4*, 552–567. [CrossRef]

12. Oliver, E.A. Critical Assessment 23: Gallium nitride-based visible light-emitting diodes. *Mater. Sci. Technol.* **2016**, *32*, 737–745. [CrossRef]
13. Boukamp, B.A.; Huggins, R.A. Lithium ion conductivity in lithium nitride. *Phys. Lett.* **1976**, *58*, 231–233. [CrossRef]
14. Drewnicka, D. Advanced investigation methods of nitride layers after heat treatment. *Inżynieria Powierzchni (Surf. Eng.)* **2012**, *2*, 14–18.
15. Borsa, D.M. Nitride-based Insulating and Magnetic thin Films and Multilayers. Available online: [https://www.rug.nl/research/portal/en/publications/nitridebased-insulating-and-magnetic-thin-films-and-multilayers\(a667d5ad-8d0b-4eda-80c7-130ef5315665\).html](https://www.rug.nl/research/portal/en/publications/nitridebased-insulating-and-magnetic-thin-films-and-multilayers(a667d5ad-8d0b-4eda-80c7-130ef5315665).html) (accessed on 10 March 2004).
16. Yamashita, S.; Masubuchi, Y.; Nakazawa, Y.; Okayama, T.; Tsuchiya, M.; Kikkawa, S. Crystal structure and magnetic properties of “ α ”-Fe₁₆N₂ containing residual α -Fe prepared by low-temperature ammonia nitridation. *J. Solid State Chem.* **2012**, *194*, 76–79. [CrossRef]
17. Xiong, X.C.; Redjaïmia, A.; Gouné, M. Transmission electron microscopy investigation of acicular ferrite precipitation in γ' -Fe₄N nitride. *Mater. Charact.* **2010**, *61*, 1245–1251. [CrossRef]
18. Buschow, K.H.J.; Robert, W.; Cahn, P.V. *Encyclopedia of Materials: Science and Technology*; Elsevier Ltd.: Amsterdam, The Netherlands, 2001.
19. Lengauer, W.; Eder, A. *Nitrides: Transition Metal Solid-State Chemistry, Encyclopedia of Inorganic Chemistry*, 2nd ed.; King, R.B., Ed.; John Wiley & Sons, Ltd.: Chichester, UK, 2005; Volume VI, pp. 3515–3531.
20. Litasov, K.D.; Shatskiy, A.; Ponomarev, D.S.; Gavryushkin, P.N. Equations of state of iron nitrides ϵ -Fe₃N_x and γ -Fe₄N_y to 30 GPa and 1200 K and implication for nitrogen in the Earth’s core. *J. Geophys. Res. Solid Earth* **2017**, *122*, 3574–3584. [CrossRef]
21. Jegoua, S.; Barrallier, L.; Kubler, R. Phase transformations and induced volume changes in a nitrided ternary Fe–3%Cr–0.345%C alloy. *Acta Mater.* **2010**, *58*, 2666–2676. [CrossRef]
22. Runge, J.M.; Pomis, A.J. Presented at the XII Ebrats Brazilian Surface Treatment Meeting and II Latin—American Interfinish, Sao Paulo, Brazil, 10 May 2006.
23. Kugler, G.; Vecko-Pirtovsek, T.; Tercelj, M. Wear behaviour of nitrided microstructures of aisi h13 dies for hot extrusion of aluminium. *Metallurgija* **2006**, *45*, 21–29.
24. Liapina, T.; Mittemeijer, E.J.; Leineweber, A.; Knapp, M. γ' -Fe₄N formation in decomposing ϵ -Fe₃N: A powder diffraction study using synchrotron radiation. *Z. FÜR Krist. Suppl.* **2006**, *23*, 449–454. [CrossRef]
25. Available online: <https://www.alliedmarketresearch.com/aluminium-market> (accessed on 20 December 2019).
26. Available online: https://www.grupakety.com/Media/files/PROGNOZA_3.pdf (accessed on 8 February 2019).
27. Steiner, T.; Mittemeijer, E.J. Alloying element nitride development in ferritic Fe-based materials upon nitriding: A review. *J. Mater. Eng. Perform.* **2016**, *25*, 2091–2102. [CrossRef]
28. Clarke, S.J. *Encyclopedia of Materials: Science and Technology*; Buschow, J.K.H., Cahn, R.W., Veyssiere, P., Flemings, M.C., Eds.; Elsevier Ltd.: Amsterdam, The Netherlands, 2001.
29. Farault, G.; Gautier, R.; Baker, C.F.; Bowman, A.; Gregory, D.H. Crystal Chemistry and Electronic Structure of the Metallic Ternary Nitride, SrTiN₂. *Chem. Mater.* **2003**, *15*, 3922–3929. [CrossRef]
30. Fromhold, A.T., Jr. Fundamental Theory of the Growth of Thick Oxide Films on Metals. *J. Phys. Soc. Jpn.* **1980**, *48*, 2022–2030. [CrossRef]
31. Roosendal, S.J. Passivation Mechanisms in the Initial Oxidation of Iron by Oxygen and Water Vapor. Ph.D. Thesis, University Utrecht, Utrecht, Netherlands, 1999.
32. Chemical kinetics. In *Reactions of Solids with Gases*; Bamford, C.H.; Tipper, C.F.H.; Compton, R.G. (Eds.) Elsevier: Amsterdam, The Netherlands; Oxford, UK; New York, NY, USA; Tokyo, Japan, 1984; Volume 21.
33. Li, Y.; Wang, L.; Zhang, D.; Shen, L. The effect of surface nanocrystallization on plasma nitriding behaviour of AISI 4140 steel. *Appl. Surf. Sci.* **2010**, *256*, 4149–4152. [CrossRef]
34. Castro Munoz, A.E.; Piedad-Beneitez, A.; Valencia-Alvarado, R.; López-Callejas, R.; Mercado-Cabrera, A.; Pena-Eguiluz, R.; Rodriguez-Mendez, B.G. The Corrosion Enhancement due to Plasma Post-Oxidation Subsequent to Plasma Nitriding of a Steel AISI 4140. *Acta Phys. Pol.* **2015**, *128*, 824–827. [CrossRef]
35. Cao, Y.; Norell, M. Role of Nitrogen Uptake During the Oxidation of 304L and 904L Austenitic Stainless Steels. *Oxid. Metals* **2013**, *80*, 479–491. [CrossRef]
36. Yuan, X.; Zhao, Y.; Li, X.; Chen, L. Effects of gas nitriding temperature on the surface properties of a high manganese TWIP steel. *Metals* **2017**, *7*, 102. [CrossRef]

37. Ertl, G.; Huber, M. Interaction of Nitrogen and Oxygen on Iron Surfaces. *Z. Fur Phys. Chem. Neue Folge* **1980**, *119*, 97–102. [[CrossRef](#)]
38. Kniep, R. Ternary and quaternary metal nitrides: A new challenge for solid state chemistry. *Pure Appl. Chem.* **1997**, *69*, 185–191. [[CrossRef](#)]
39. Steiner, T.; Meka, S.R.; Bischoff, E.; Waldenmaier, T.; Mittemeijer, E.J. Nitriding of ternary Fe–Cr–Mo alloys; role of the Cr/Mo-ratio. *Surf. Coat. Technol.* **2016**, *291*, 21–33. [[CrossRef](#)]
40. Tacikowski, J.; Wach, P.; Michalski, J.; Burdyński, K. Separation hardening by heat treatment of nitrided carbon steel. *Mater. Eng.* **2014**, *6*, 552–555.
41. Andrzejewska, E.; Gonzalez-Arrabal, R.; Borsa, D.; Boerma, D.O. Study of the phases of iron–nitride with a stoichiometry near to FeN. Nucl. Instrum. Methods Phys. Res. Sect. B Beam Interact. *Mater. At.* **2006**, *249*, 838–842. [[CrossRef](#)]
42. Orlik, R.; Ratajski, J.; Suszko, T.; Michalski, J.; Dobrodziej, J.; Gilewicz, A. Precise shaping of phase structure and thickness of nitrided layer on the example of dies for pressure casting of aluminium. *Surf. Eng.* **2009**, *3*, 15–20.
43. Xu, C.H.; Gao, W. Pilling-Bedworth ratio for oxidation of alloys. *Mater. Res. Innov.* **2000**, *3*, 231–235. [[CrossRef](#)]
44. Dwivedi, D.; Lepková, K.; Becker, T. Carbon steel corrosion: A review of key surface properties and characterization methods. *RSC Adv.* **2017**, *7*, 4580–4610. [[CrossRef](#)]
45. Melchers, R.E. Predicting long-term corrosion of metal alloys in physical infrastructure. *NPJ Mater. Degrad.* **2019**, *3*, 1–17. [[CrossRef](#)]
46. Mao, W.; Ma, Y.; Sloof, W.G. Internal Oxidation of Fe–Mn–Cr Steels, Simulations and Experiments. *Oxid. Metals* **2018**, *90*, 237–253. [[CrossRef](#)]



© 2020 by the authors. Licensee MDPI, Basel, Switzerland. This article is an open access article distributed under the terms and conditions of the Creative Commons Attribution (CC BY) license (<http://creativecommons.org/licenses/by/4.0/>).